Self-oscillatory Flows near Blunted Bodies, Giving off Opposite Jets: CFD Study

V. I. Pinchukov

SD of Russian Academy of Sc., In-te of Computational Technologies, Novosibirsk, Russia

Abstract - ***Numerical investigations of self-oscillatory compressible flows are carried out. Unsteady regimes are supposed to be resulted from resonance interactions of "active" elements of flows. Hypothesis is used that contact discontinuities and intersection points of shocks with shocks or shocks with contact discontinuities compose the flow set of "active" elements. Two-dimensional Reynolds-averaged Navier-Stocks equations added by an algebraic turbulence model are solved by the implicit third order Runge-Kutta scheme. The turbulent viscosity is defined by the Prandtl formulae, which deals with the turbulent length scale calculated on the base of the generalized Karman formulae. Calculations of the open cavity flow are used to verify the turbulence model. Self-oscillatory compressible flows near blunted bodies, giving off supersonic opposite jets from forehead surfaces, are studied numerically.***

Index terms - **Reynolds-averaged Navier-Stocks equations, Runge-Kutta scheme, Self-oscillatory flows.**

I. INTRODUCTION

Main purpose of the recent paper is to study jet unsteady flows by means of numerical calculations. A jet cavity interaction (see [1]-[5]) and a jet impinging on a plate [6]-[14] are known to have self-oscillatory regimes. Flows near blunted bodies (cylinders or cones), giving off opposite jets, were discovered to have unsteady regimes [14],[15]. Here these investigations are continued. New model of turbulence is used in flow calculations.

Flow self-oscillations are supposed to be resulted from resonance interactions of flow "active" elements, namely, elements, which amplify disturbances. The hypothesis is formulated in [13]-[15] that contact discontinuities and intersection points of shocks with shocks or shocks with contact discontinuities compose the flow set of "active" elements. Possibility of the disturbances amplification by contact discontinuities is a result of the Kelvin-Helmholtz instability and is accepted. Inclusion of intersection points to a list of amplifiers [13]-[15] is initiated by the known possibility to operate types of the shock reflection from a plane (Mach or

regular type) by small influences. If small influences yield significant change of the flow in the reflection zone, then this flow structure is an amplifier of disturbances. Possibility of any intersection points of discontinuities (intersection lines in 3d case) to amplify disturbances is used here as a hypothesis, which is checked by results of a search for new unsteady flows. A search for new unsteady flows is carried out by investigations of flows, containing "active" elements. The third order implicit method [16] us used.

Recent flows calculations show that some unsteady solutions may exist if Euler equations are used for the flow description, but these solutions are transforming to steady state solutions if a turbulence model is used and if "level" of turbulence is sufficiently high. This paper is devoted to a search for flows which are unsteady in both approaches.

II. THE KARMAN MODEL OF TURBULENCE

A search for new self-oscillatory flows is based on trial calculations of numerous different flows. So, there is necessity in a simple and universal turbulence model. The algebraic model of turbulence is used in [13]-[15], based on the Prandtl formulae $\mu = \rho/w|z^2$, where w is vorticity, ρ is density, $z=kl$, l is the turbulent length scale, $k=0.4$ is the Karman coefficient. This formulae is dealt in classical Cebeci-Smith and Baldween-Lomax models, where the length scale is defined as a distance the recent point to the solid wall. The Prandtl formulae is used also in the Smagorinsky model of LES (Large Eddy Simulation), where the length scale is the grid cell size. Another definition is used in [13]-[15]. The turbulent length scale is calculated as a distance of recent point to the nearest zero vorticity zone. These zones are defined by checking of some inequality, which deals with velocity circulations for grid sells.

More convenient procedure is used here. The distance l of recent point x to the zero point of any one dimensional function f(x) may be calculated approximately by the formulae

$l \approx$ f(x)/(df(x)/dx). Extension of this formulae to the 2D case is evident:

$l \approx$ f(x,y)/|grad f(x,y)|,   (1)

where grad f(x,y) – vector $(\partial f/\partial x, \partial f/\partial y)$, |grad f(x,y)|=

$[(\partial f/\partial x)^2 + (\partial f/\partial y)^2]^{1/2}$.

The idea of recent model is to use this formulae for the case f=w, w - vorticity. The Karman model, which is applied in the theory of a turbulent boundary layer, deals with the modified formulae (1), namely,
z=k w/$(\partial w/\partial y) \approx k \partial u/\partial y /(\partial^2 u/\partial y^2)$.

This modification is resulted from evaluations w(x,y) $\approx \partial u/\partial y$, |grad w| $\approx |\partial^2 u/\partial y^2|$, which are true in the case of boundary layer. Since the boundary layer approach is not used here, the formulae (1) should be considered. Of course, this formulae gives bad results in regions with "small" values of |grad w(x,y)| and so should be modified. Next three step procedure of turbulent viscosity calculations is used here:

1. l=/w|/[|grad w|^2 +δ(|grad u|^2 + |grad v|^2)/Det]$^{1/2}$,

     z=lk/(1+l^4 /λ^4 27/256), μ_0 =ρ|w|z^2 ,

k =0.4– the Karman coefficient, λ - the delimiting parameter, which allows to vary "level" of turbulence, u,v – velocity components, δ =0.01- the coefficient, providing regularity of written above formulas in the case grad w $\approx$ 0, Det=∂ x/$\partial \xi \times \partial$ y/∂ η- ∂ x/∂ η$\times \partial$ y/$\partial \xi$, ξ, η – transformed variables**.**

2. $\mu_1 = \int_{-m\Delta x}^{m\Delta x}$ μ_0 (x+ς,y) Ω (m Δx,ς)dς,

3**.** $\mu_{tur} = \int_{-m\Delta y}^{m\Delta y}$ μ_1 (x,y+ς) Ω (m Δy, ς)dς,

Ω (ε ,ς)= (1- ς^2 /ε^2)$^{1/2}$ /$\int_{-\varepsilon}^{\varepsilon}$ (1- ς^2 /ε^2)$^{1/2}$ dς**.**

The first step of this procedure defines the local turbulent length scale, which approximates the Karman formulae near boundaries of "ideal" zones with small vorticity (here the relation l/λ is small). Increasing of this relation leads to tur-

bulent length scale increasing till the maximal value (if regularization coefficient δ is equal to zero, this maximal value is kλ), then this scale decreases and tends to the zero limit. The turbulent length scale decreasing is intended to provide low level of the turbulent viscosity inside of circulation zones. Open cavity flow calculations allow to prove that turbulent viscosity is really much smaller in the middle of large circulation zones then viscosity near boundaries of these zones.

Second and third steps are devoted to averaging of the turbulent viscosity. This averaging provides "smoothing" of turbulent viscosity and, consequently, improves convergence to steady state solutions and prevents false unsteadiness. Averaging is divided into two stages to diminish the computational cost of the procedure. The averaging region is defined by the integer parameter m, which is chosen as m=7.

This model is universal and may be used for larger values of the parameter λ, then the previous model [13]-[15]. Of course, this model is too simple to give exact results for any turbulent flows. So the delimiting parameter λ is choosing to be sufficiently small to avoid errors resulted from too primitive model of turbulence. The purpose of usage of this model is to find flows, which keep unsteady regimes when the delimiting parameter λ is increasing, but remains much less then geometrical lengths of problems. It should be noted that boundary conditions of "ideal" type are used on solid walls in the case of RANS, namely, zero value of normal velocity and extrapolation relations for all other variables are used as boundary conditions. So, if to tend the delimiting parameter λ to the zero limit, numerical flow fields tend to the solution of Euler equations. Thus this turbulence model may be considered as a tool to take into consideration influence of turbulent dissipation on solutions of Euler equations for low levels of turbulence.

Naturally, numerical calculations deal with dimensionless variables. These variables are defined as relations of initial variables and next parameters of the undisturbed flow or the body size: p_∞ - for pressure, ρ_∞ - for density, $\sqrt{p_\infty/\rho_\infty}$ - for velocity, r (blunt radiuses of cones or cylinders) – for space variables, $r/\sqrt{p_\infty/\rho_\infty}$ - for time.

III. TEST PROBLEMS
The supersonic flow resulted from interaction of two parallel uniform streams (see fig. 1) is calculated on the base of Euler and RANS equations with usage of written above turbulence model. The flow is defined by upper stream pa-

rameters p^u =1, ρ^u =1, M^u =2.4 and down stream parameters p^d =0.25, ρ^d =0.5, M^d =4. The 180×135 grid is used. Fig. 1 shows the density distribution for the case μ_{tur} =0.
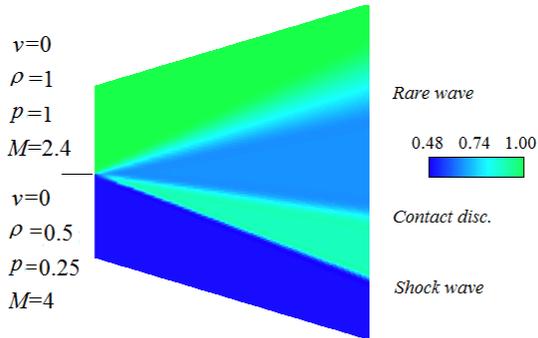

Fig. 1. Interaction of two ideal parallel streams, the density distribution

Fig. 2 represents results of flow calculations for the turbulent case. The delimiting parameter λ=0.075L (L - the left boundary size) is used. Turbulent Reynolds number Re=L $u^d \rho^d$ /max$_{ik}$ (μ_{tur}) of 88 is resulted. Calculations are carried out for CFL number 1.38. Fig. 2(a) shows convergence histories, 1- the ideal case μ_{tur}=0, 2 – the turbulent case, 3 – turbulent viscosity is calculated without averaging, steps 2 and 3 are omitted. So, convergence histories show, that averaging is important part of the recent turbulent model. Fig 2(b) shows the density distribution for the turbulent flow. If to compare figs. 1 and 2(b), difference is seen only in the zone of contact discontinuity. Quick convergence of method [16] is seen in fig. 2(b) for the CFL number 1.38. But since increasing of CFL numbers leads to increasing of computation errors, recent self-oscillatory flows investigations are carried out for CFL numbers within limits 0.5 – 1.
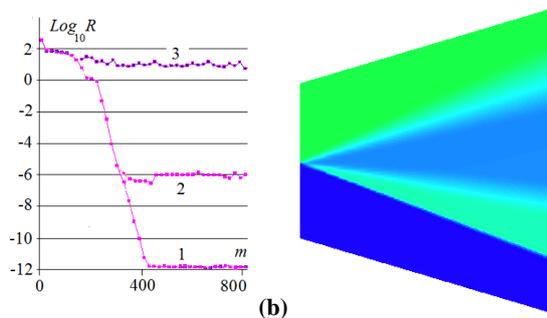

Fig. 2. Supersonic streams interaction, (a) - convergence histories, (b) – the density distribution.

An open cavity flow [17]-[18] is calculated with usage of the Karman turbulence model. The flow geometry is defined by parameters d=5.2mm (the cavity depth, see fig. 3), L=10.4mm (the cavity length), the numerical region above cavity has the height of 10.4mm and the length of 20.8mm. This cavity flow is tested numerically with flow field condi-

tions M_∞ =2, θ = 0.979mm (momentum thickness of the boundary layer on the inflow plane). Boundary conditions for computations are no-slip adiabatic wall on solid surfaces, extrapolations on the outflow boundaries, prescribed variables on the inflow plane. Namely, dimensionless pressure and density are 1, the radial velocity v is 0, the horizontal velocity is $u = M_\infty \sqrt{\gamma} (2\sqrt{s} - s)$ if $s=y/\theta \leq 10$, $u = M_\infty \sqrt{\gamma}$ if $s=y/\theta > 10$, γ =1.4 – the specific heat ratio. So, boundary conditions of "viscous" type are used here, while recent approach is intended for "ideal" boundary conditions. Nevertheless presented below numerical results allow to evaluate the approach accuracy.

Fig. 3(a) shows the 44×52 mesh (grid compression $\Delta x^{max} / \Delta x^{min} \approx \Delta y^{max} / \Delta y^{min} \approx 10$), fig. 3(b) shows flow streamlines. The delimiting parameter λ=0.07d is used. The turbulent Reynolds number Re= $\rho_\infty u_\infty d$/max$_{ik}$ (μ_{tur})= =180 is resulted. Calculations are carried out for CFL number 0.97, the 561×533 mesh is used.
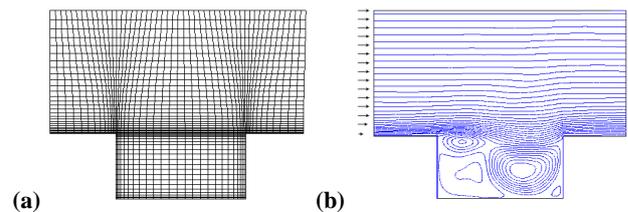

Fig. 3. The open cavity flow, (a) – the 52×44 mesh, (b) – flow streamlines (the 561×533 mesh)

The time history of the surface pressure at the $x=2L/3$ point on the cavity floor is used to form the time averaged sound pressure level $\overline{SPL}$, which is computed by the equation

$$\overline{SPL} = 10 \, Log_{10} (\overline{p'^2} / p_{ref}^2),$$

where $\overline{p'^2} = \sum_n (p_n - \overline{p})^2 /N$, p_{ref} =20mkPa/ p_∞,

p_∞ =98066Pa (the air pressure under normal conditions) is used since dimensionless variables are dealt here. The resulting time averaged $\overline{SPL}$ of 175.9Db may be compared with the numerical $\overline{SPL}$ of 167.54Db and the

experimental $\overline{SPL}$ of 164.41Db presented in [17]. The weighted $\overline{SPL}$ for data from various sources [18] is approximately 171Db.

IV. FLOWS NEAR BLUNTED BODIES

Investigations of unsteady interactions of uniform supersonic streams with blunted cones, giving of opposite supersonic jets, were began in [14],[15] and are continued here. Calculated flow fields allow to see shocks, contact discontinuities and intersection points. So, these flows may be waited to produce self-oscillations, according to the proposed mechanism of the flow unsteadiness.

Boundary conditions for computations are zero value of the normal velocity and extrapolation relations for all other variables on the body surface, extrapolations on the outflow boundary at right side of fig. 4, prescribed variables on the inflow forehead boundary and on the spherical boundary, corresponding to the opposite jet, zero value of the radial velocity and extrapolations on symmetry axes.

Fig. 4 shows density levels for the steady flow near the spherically blunted cylinder. The conical supersonic jet is running out from a point source located at the sphere centre. Calculations are carried out with flow conditions $δ_{jet}$ =arcsin(2/3) (the jet half-angle), M_{jet} =4.5 (jet Mach number on the spherical surface), p_{jet} =0.23254$p_∞$, $ρ_{jet}$ =0.46455$ρ_∞$. There are two shock waves, namely, the shock wave on the left side of fig. 4, which brakes an outer stream, and the second shock wave closer to the spherical blunt, which brakes a jet, the extended contact discontinuity between them (denoted by the arrow 1), and the second contact discontinuity, corresponding to the jet boundary. The intersection point (denoted by the arrow 2) of this discontinuity with the shock acts as an amplifier of perturbations. It is important to note that the new contact discontinuity starts from this point and propagates to the region at right side of fig. 4**.** The contact discontinuity, signed by the arrow 1, also propagates to this region.

So, if some flow contains the tail shock, this shock crosses

both contact discontinuities, consequently, two new intersection points appear. All these intersection points may interact one with another or with the body surface and, consequently, may generate self-oscillations.
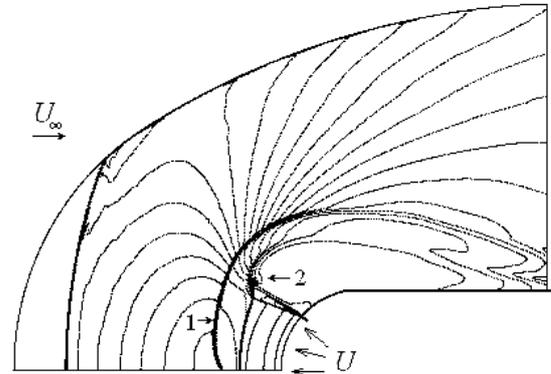

Fig. 4. The blunted cylinder, density levels.

Fig. 5 shows the density distribution for the flow, defined by parameters: $δ_{jet}$ = arcsin(1/3), $M_∞$ =1.3, M_{jet} =4.5, p_{jet} =0.23254$p_∞$, $ρ_{jet}$ =0.46455$ρ_∞$. The 590×544 mesh is used. The delimiting parameter $λ=r_{bl}/30$ (r_{bl} - the bold sphere radius) is chosen. This choice results the Reynolds number Re= $ρ_∞ u_∞ r_{bl}/max_{ik}(μ_{tur})$ =97. The density distribution (see fig. 5) shows shock waves moving from the body bold region to the main forehead shock wave.
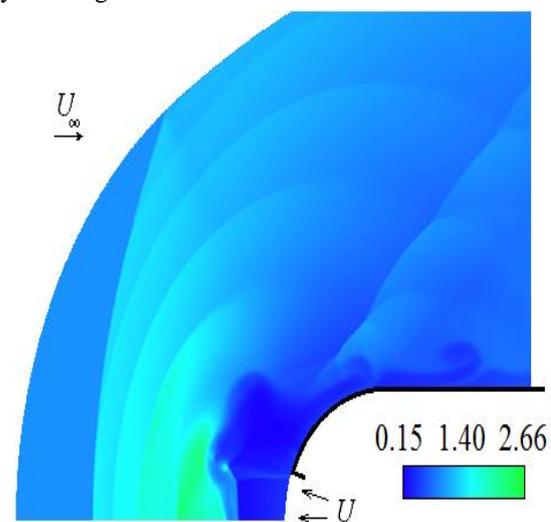

Fig. 5. The density distribution near the blunted cylinder

Fig. 6 shows the density history at the interface point of spherical and cylindrical parts of the body. It may be seen that this history is nearly periodical with the T=7.5 period.
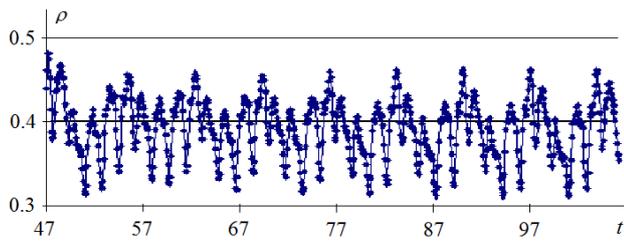
Fig. 6. The density history, M_∞ =1.3.

To show flow dynamics through this time period density distributions at time moments $t=t_0$ +nT/4, n=1…4, t_0 =107.0, T=7.5, are presented in fig. 7.
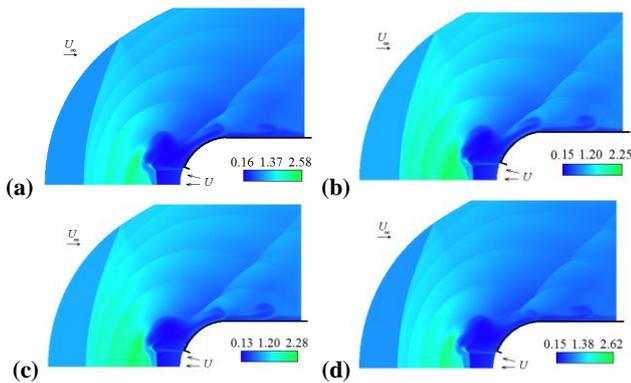

(a)   **(b)**

(c)   **(d)**

Fig. 7. Density distributions, (a) – $t=t_0$ +T/4, (b) – $t=t_0$ + +T/2, (c) - $t=t_0$ +3T/4, (d) – $t=t_0$ +T.

It is easy to see that fig. 5, which shows the density distribution at the time moment $t= t_0$ =107.0, and fig. 7© are like, so these figs. show nearly periodical dynamics of the considered unsteady flow.

The flow near blunted cone with half-angle 15° is studied numerically with flow conditions M_∞ =1.2, M_{jet} =4, p_{jet} =0.29167p_∞ , ρ_{jet} =0.46875ρ_∞ , δ_{jet} =arcsin(1/3). Calculations are carried out for three values of the delimiting parameter λ: $\lambda=r_{bl}$/30, $\lambda=r_{bl}$/20, $\lambda=r_{bl}$/15 (r_{bl} - radius of the sphere at the top of the cone). Figs. 8, 9 show numerical results for $\lambda=r_{bl}$/15. This value of the parameter λ results the Reynolds number Re= $\rho_\infty u_\infty r_{bl}$ /max_{ik} (μ_{tur}) =131. Self-oscillatory regimes with nearly the same amplitude of oscillations (see fig. 9) are observed for all these values of parameter λ.

The density distribution is shown in fig. 8. Shock waves moving from the region near the body bold to the main forehead shock wave and vortexes appearing near the body bold and moving downstream along the cone are seen in this fig.
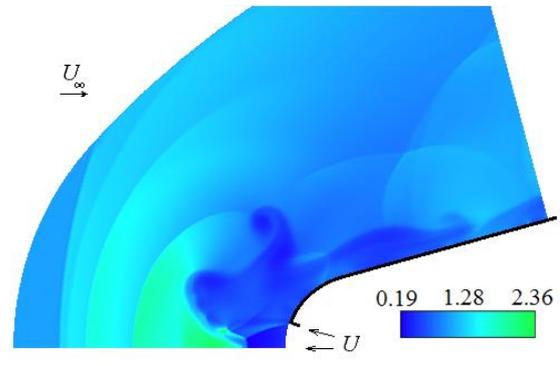

Fig. 8. The density distribution, M_∞ =1.2.

Fig. 9 shows the density history at the interface point of spherical and conical parts of the body.
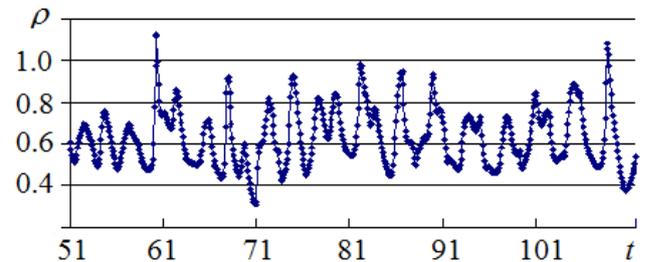

Fig. 9. The density history, M_∞ =1.2.

V. CONCLUSIONS

Recent paper is devoted to continuation of numerical search for unsteady flows, started in [13]-[15]. Interactions of supersonic streams with blunted bodies, giving off supersonic jets are investigated. These flows contain several "active" elements, so unsteady regimes are possible according to the written above hypothetical mechanism of self-oscillations. Intensive flow self-oscillations are seen in numerical investigations. But it is unclear which elements are responsible for main interactions, producing self-oscillatory regimes.

The generalized Karman model of turbulence, presented here, allows to filter unsteady solutions and to found flows with self-oscillatory regimes which existence does not depend on usage of RANS or Euler equations. Such flows are found here only for outer stream Mach numbers $M_\infty \leq 1.3$.

The initial stage of investigations of this problem is presented in [14]-[15] and here. Both CFD modelling and experimental study are necessary to get more understanding of physics of unsteady flows near blunted bodies, giving off opposite jets .

REFERENCES

[1] Kastner J., Samimy M., Development and Characterization of Hartmann Tube Fluid Actuators for High- speed Control, American Institute of Aeronautics and Astronautics J., Vol. 40 (10), 2002, 1926–1934.

[2] Raman G., Envia E., Bencic T.J., Jet Cavity Interaction Tones, American Institute of Aeronautics and Astronautics J., Vol. 40 (8), 2002, 1503–1511.

[3] Sarpotdar S., Raman G., Cain A.B., Powered Resonance Tubes: Resonance Characteristics and Actuation Signal Directivity, Experiments in Fluids Vol. 39 (6), 2005, 1084–1095.

[4] Raman G., Khanafseh S., Cain A.B., Kerschen E., Development of High Band Width Powered Resonance Tube Actuators with Feedback Control, J. of Sound and Vibration 269 (3–5), 2004, 1031-1062.

[5] Murugappan S., Gutmark E., Parametric Study of the Hartmann–Springer Tube, Experiments in Fluids, Vol. 38 (6), 2005, 813–823.

[6] Henderson B., Bridges J. Wernet, M. An Experimental Study of the Oscillatory Flow Structure of Tone-Producing Supersonic Impinging Jets, J. Fluid Mech., Vol. 542, 2005, 115–137.

[7] Kuo C.-Y., Dowling A. P. Oscillations of a Moderately Underpanded Choked Jet Impinging Upon a Flat Plate, J. Fluid Mech., Vol. 315, 1996, 267–291.

[8] Berland J., Bogey C., Bailly C. Numerical Study of Screech Generation in a Planar Supersonic Jet, Phys. Fluids, Vol. 19, 2007, 75-105.

[9] Sakakibara Y., Iwamoto J. Numerical Study of Oscillation Mechanism in Under expanded Jet Impinging on Plate, J. Fluids Eng. , Vol. 120, 1998, 477.

[10] Bodony D. J., Lele S. K. On Using Large-Eddy Simulation for the Prediction of Noise from Cold and Heated Turbulent Jets, Phys. Flids , Vol. 17, 2005.

[11] Bogey C., Bailly C. Computation of a High Reynolds Number Jet and its Radiated Noise Using Large Eddy Simulation Based on Explicit Filtering, Comput. Fluids, Vol. 35, 2006, 1344-1358.

[12] Cheng T., Lee K. Numerical Simulations of Underexpanded Supersonic Jet and Free Shear Layer Using WENO Schemes, Int. J. Heat Fluid Flow, Vol. 26(5), 2005, 755–770.

[13] Pinchukov V. I., Numerical Modeling of Unsteady Flows with Transient Regimes, Comput. Mathem. and Mathem.Physics, Vol. 49 (10), 2009, 1844–1852.

[14] Pinchukov V. I., Modeling of Self-Oscillations and a Search for New Self-Oscillatory Flows, Mathematical Models and Computer Simulations, Vol. 4(2), 2012, 170–178.

[15] Pinchukov V. I Numerical Simulations of Self-oscillatory Flows near Blunted Bodies, Giving off Opposite Jets // Intern. J. of Mechanical Engineering and Applications - Vol. 2, No. 1, 2014, pp. 5-10.

[16] Pinchukov V. I., Numerical Solution of the Equations of Viscous Gas by an Implicit Third Order Runge–Kutta Scheme, Comput. Mathem. and Mathem. Physics, Vol. 42(6), 2002, 898-907.

[17] Tam C.-J., Orkwis P.D., Disimile P.J. Algebraic Turbulence Model Simulations of Supersonic Open-Cavity Flow Physics, AIAA J., Vol. 34(11), 1996, 2255- 2260.

[18] Tam C.-J., Orkwis P.D., Disimile P.J. Comparison of Balwin-Lomax Turbulence Models for Two-Dimensional Open-Cavity Calculations, AIAA J., Vol. 34(3), Technical Notes, 1996, 629- 632.